

Strong RR Lyrae excess in the Hercules-Aquila Cloud

Iulia T. Simion^{1*}, Vasily Belokurov¹, Mike Irwin¹, Sergey E. Koposov^{1,2}

¹*Institute of Astronomy, Madingley Rd, Cambridge, CB3 0HA,*

²*Moscow MV Lomonosov State University, Sternberg Astronomical Institute, Moscow 119992, Russia*

Accepted 2014 January 16. Received 2014 January 15; in original form 2013 December 16

ABSTRACT

We map the large-scale sub-structure in the Galactic stellar halo using accurate 3D positions of $\sim 14,000$ RR Lyrae reported by the Catalina Sky Survey. In the heliocentric distance range of 10–25 kpc, in the region of the sky approximately bounded by $30^\circ < l < 55^\circ$ and $-45^\circ < b < -25^\circ$, there appears to be a strong excess of RRab stars. This overdensity, peaking at 18 kpc, is most likely associated with the so-called Hercules-Aquila Cloud, previously detected using Main Sequence tracers at similar distances in the Sloan Digital Sky Survey data. Our analysis of the period-amplitude distribution of RR Lyrae in this region indicates that the HAC is dominated by the Oosterhoff I type population. By comparing the measured RR Lyrae number density to models of a smooth stellar halo, we estimate the significance of the observed excess and provide an updated estimate of the total luminosity of the Cloud’s progenitor.

Key words: Galaxy: structure – Galaxy: stellar content – Galaxy: halo – stars: variables: RR Lyrae – galaxies: individual: Milky Way – galaxies: photometry.

1 INTRODUCTION

With the recent discoveries of both ongoing disruption events (such as the Sagittarius stream, see e.g. Majewski et al. 2003) and of the remnants of past mergers (e.g. the Virgo Cloud, see Duffau et al. 2006; Jurić et al. 2008), there is now little doubt that a substantial portion of the Galactic stellar halo has been accreted. Today, the focus has shifted to finding out what exactly fell onto the Milky Way and when. The reconstruction of the stellar halo accretion history necessarily involves brushing away the Galactic in-situ components so that the faint fragments of broken satellites can be pieced together. Therefore, the majority of the detections of stellar halo sub-structure have been limited to high ($|b| > 30^\circ$) Galactic latitudes, where disk/bulge contamination is minimal.

The current tally (see e.g. Belokurov 2013) indicates that as much as 50% – 70% of the stellar halo is in well-mixed, seemingly smooth components, with another 30%, or perhaps even 50%, contributed by four structures: the Sagittarius stream, the Galactic Anti-centre Stellar Structure (GASS), the Virgo Cloud (containing the Virgo Overdensity and the Virgo Stellar Stream), and the Hercules-Aquila Cloud (HAC). However, curiously two of the four most massive structures in the stellar halo seem to reside very close to the disk plane. The GASS covers a large region of the low-latitude sky approximately in the direction of the anti-centre and the HAC is hidden behind the disk

and the bulge, on the other side of the Galaxy (Belokurov et al. 2007). Given their obvious proximity to the plane, claims have been made as to the genesis of these structures, linking them to perturbations in the stellar disk density. For example, Larsen et al. (2011) argue that while the excess of faint Main Sequence (MS) stars around the HAC position is real, the distance to the sub-structure was over-estimated and the true location of the Cloud is much closer, only 1 to 6 kpc from the Sun rather than 10 to 20 kpc.

The HAC is a challenging structure to map. Its presence is easily spotted due to the obvious asymmetry in the faint MS density in the directions towards the Galactic center. However, characterizing its full extent is far from straightforward. The Sloan Digital Sky Survey (SDSS) data, which provides the deepest wide area view of the sky, is not symmetric between positive and negative Galactic longitudes and latitudes. Moreover, the contiguous coverage stops at latitudes $|b| \approx 30^\circ$, but there exist some limited SDSS imaging data along several $\sim 2.5^\circ$ wide stripes slicing through the Galaxy at constant l at $|b| < 30^\circ$. The analysis of these slices (Belokurov et al. 2007) clearly indicates that the HAC signal continues to low latitudes, at least as low as $|b| \sim 15^\circ$. In addition, the Cloud is noticeably asymmetric with respect to the disk plane, i.e. at $l \sim 50^\circ$, there exists a prominent over-abundance of MS stars in the Galactic Southern hemisphere. The MS stars contributing to the over-density are in a wide magnitude range $18 < i < 22$, thus giving only an approximate indication of the distance to the Cloud.

RR Lyrae are an ideal tracer population to pin down the distance and the luminosity of the HAC. To this end,

* email: isimion@ast.cam.ac.uk

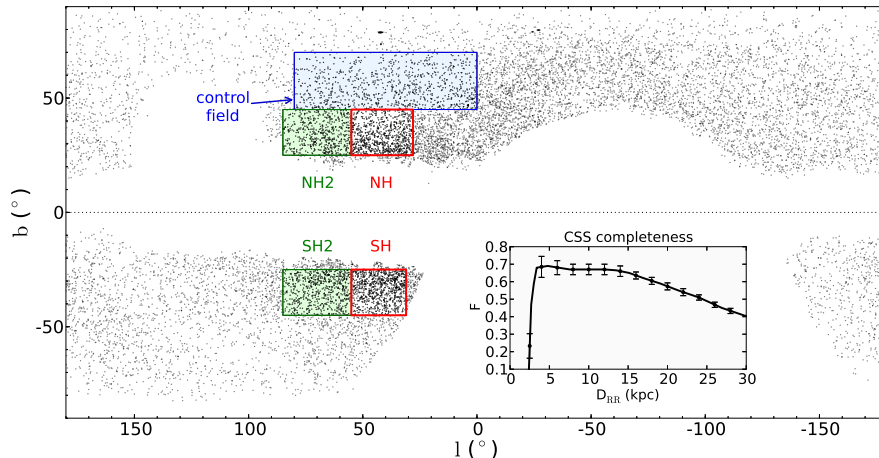


Figure 1. Spatial distribution of Catalina Schmidt Survey RRab Lyrae (DR13a) in Galactic coordinates. We highlight with blue our selection of the control field (see Section 3), with red our selections of the ‘on-cloud’ fields, in the Northern Hemisphere (NH) and in the Southern Hemisphere (SH) (see Section 4). In green we show another field selection (NH2 and SH2) that we will use in Section 4. The insert shows the completeness of the survey as a function of distance, assuming $A_V = 0$.

Watkins et al. (2009) and Sesar et al. (2010) exploit the multi-epoch data in the narrow equatorial SDSS Stripe 82 to detect RR Lyrae stars with high efficiency. Stripe 82 briefly crosses the HAC region in the South and both teams report a significant overdensity of RR Lyrae at $45^\circ < l < 60^\circ$ and $-45^\circ < b < -25^\circ$. Watkins et al. (2009) give the distance to the HAC of 22 kpc, this is the average over the cross-section of the Cloud and the Stripe.

In this work, we take advantage of the large sample (in excess of 10,000) of intermediate distance (5-30 kpc) RR Lyrae stars of the *ab* type detected by the Catalina Real-time Transient Survey (CRTS). The size of the sample and the distance range probed by these data is ample to search for the signatures of large-scale halo sub-structure, and in particular the HAC. The paper is structured as follows. Section 2 briefly describes the properties of the RR Lyrae dataset analysed while Section 3 describes the smooth stellar halo models used to reveal the Cloud and estimate its significance. Finally, Section 4 focuses on the properties of the RR Lyrae stars in the Cloud itself.

2 DATA

RR Lyrae are radially pulsating horizontal branch stars, with pulsation periods between 5 and 15 hours and amplitudes in the range 0.2 -1.6 mag in the *V*-band. These stars have a well defined Period-Luminosity-Metallicity relation which allows for accurate distance determination (normally with less than 10% uncertainty). RR Lyrae are low-mass, long-lived stars (typically more than 10 Gyrs old) and are found in large quantities in globular clusters and in the stellar halo of our Galaxy making them ideal tracers of the internal substructure of the Milky Way. They are sufficiently bright, with an almost invariable absolute magnitude ($M_V \approx 0.59$) meaning that they can be detected out to large distances in relatively shallow surveys, i.e. ~ 100 kpc for a survey with a modest limiting magnitude between 20 and 21 mag.

RR Lyrae are also relatively abundant, with their number density in the solar neighborhood between 4 and 6 kpc^{-3} . These tracers allow for studies of the halo substructure with good spatial resolution (e.g. Preston et al. 1991; Vivas & Zinn 2006). Several large-scale RR Lyrae surveys exist already and a useful comparison between them in terms of their sky coverage and completeness is presented in Table 1 of Mateu et al. (2012). However, 2013 saw two new RR Lyrae catalogues published: LINEAR II (Sesar et al. 2013) which probes distances between 5 kpc and 30 kpc over $\sim 8,000 \text{ deg}^2$; and the Catalina Schmidt Survey (Drake et al. 2013a,b, hereafter DR13a,b) reaching distances between 2 and 60 kpc over $\sim 20,000 \text{ deg}^2$ of the sky.

The Catalina Sky Survey began in 2004 and used three different telescopes to discover near-Earth objects (NEOs) and potentially hazardous asteroids (PHAs). Each of the survey telescopes is run as a separate sub-survey. In this work, we are using the data from the Catalina Schmidt Survey (CSS), one of the three sub-surveys of the Catalina Sky Survey. The CSS contains an impressive sample of $\sim 14,500$ type *ab* RR Lyrae with magnitudes between 11.5 and 20 mag, spread over approximately half of the sky ($0^\circ < \text{RA} < 360^\circ$, $22^\circ < \text{DEC} < 65^\circ$), the largest Galactic volume ever surveyed with RR Lyrae. The catalogue comes with reliable distance estimates from a well-studied absolute magnitude vs. metallicity distribution (Catelan & Cortés 2008).

The parameters of the CSS RRab stars are listed in Table 1 of DR13a and Table 2 of DR13b. In what follows, we are going to use their published equatorial coordinates RA, DEC, (see Figure 1), as well as the magnitudes V_0 and the heliocentric distances D_{RR} . The V_0 magnitudes are already extinction corrected using the Schlegel et al. (1998) reddening maps. The uncertainties on all of the above quantities are not listed but estimates are provided. The average metallicity of the sub-sample with available SDSS spectra is approximately -1.55 (see Figure 20, DR13a) therefore, given that the absolute magnitude of the RRL has a linear dependence on metallicity (e.g. Chaboyer 1999), we can assume $M_V \approx 0.6$ for the CSS data. The dispersion in the

Table 1. Single power-law and broken power-laws models with their parameters. The normalisation for the Watkins et al. (2009) model is divided by 11, in agreement with Sesar et al. (2010) and DR13b.

Model	α_{in}	α_{out}	r_b	q_H	ρ_{\odot}^{RR} kpc $^{-3}$	No of tracers (approx)	Area deg 2	Survey	Reference
BPL	2.40	4.50	23	1.00	3.0	316 RRab	290	Stripe 82	Watkins et al. (2009)
SPL	2.77			0.64	5.6	366 RRab	290	Stripe 82	Sesar et al. (2010)
BPL	2.30	4.60	27	0.61	7.3	6,800 BHBs	14,000	SDSS DR8	Deason et al. (2011)
BPL	2.62	3.80	28	0.71	5.9	34,000 MS	170	CFHTLS	Sesar et al. (2011)
SPL	2.42			0.63	5.6	4,000 RRab	8,000	LINEAR II	Sesar et al. (2013)

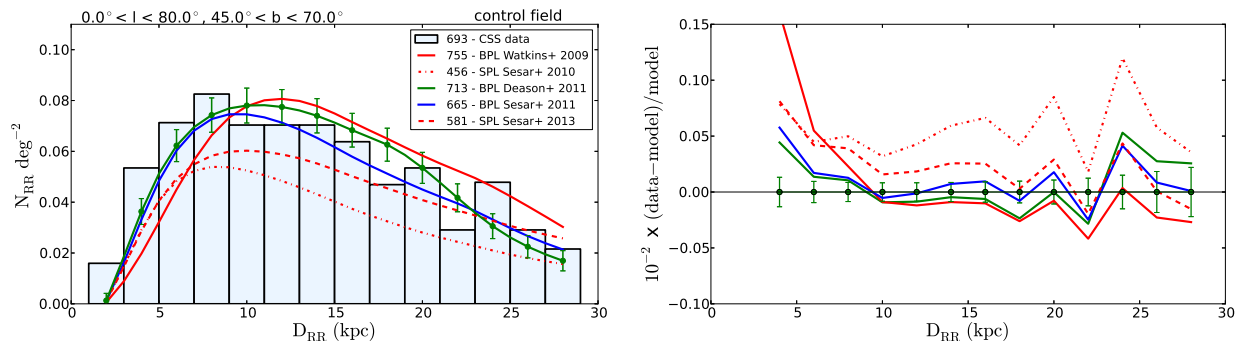


Figure 2. Left panel: Comparison between the heliocentric distance number density distribution of CSS RRab Lyrae in the control field (selected in blue in Figure 1) and five simple power law model predictions (see labels and Table 1). The numbers in the legend are the integrated number of RRab in the 5-28 kpc distance range. As our sample of RRab is incomplete, we corrected the model predictions for the effects of completeness, using equation 5. Right panel: Relative difference between the data and the model. The most suitable models for predicting the data in the control field are the Deason et al. (2011) and Sesar et al. (2011) broken power-law models (the Deason et al. (2011) model was scaled such that it reproduces the number of RRL observed in this field).

metallicity of the sub-sample, ~ 0.3 dex, introduces an error on the absolute magnitude, while the apparent magnitudes are affected by photometric error. These two factors translate into a total uncertainty on the distances of the order of 7% (e.g. at $D = 15$ kpc the error will be $\delta D \approx \pm 1$ kpc).

3 SIMPLE SMOOTH HALO MODELS

To probe the clumpiness of the Galactic RR Lyrae distribution on the scales of several kpc, a reasonable first step is to compare the observed tracer volume density to the predictions of a simple smooth halo model. To guide this comparison we identify several locations of interest in the central Galaxy. Figure 1 shows the spatial distribution of all $\sim 14,400$ RRab Lyrae in the CSS sample. The principal “on-cloud” fields in the South and North Galactic hemispheres are plotted in red and marked with NH and SH respectively, the secondary fields are marked in green. Additionally, a comparison field (control field) is chosen at suitably high Galactic latitude in the region free of known sub-structure; this appears in blue. These fields are selected with the following logic in mind. In the comparison field, a smooth density model can be found that describes the data well. In the primary “on-cloud” fields, the strength of the residuals with respect to the model can be used to ascertain the presence of the Cloud. The neighboring secondary fields, labelled NH2 and SH2, are analysed to constrain the extent of the HAC.

As illustrated in e.g. Deason et al. (2011), power law volume density models are fairly successful at predicting the

number counts of old metal-poor stars in the Galactic halo. According to these authors, within 20 kpc of the Galactic centre stellar halo substructure, as traced by BHBs, reaches the levels of 10% – 20% when the known large overdensities such as the Sagittarius stream are removed. Since, apart from the HAC, there are no other halo structures known in the region we are focusing on, it is safe to posit that similar levels of smoothness should be seen in the RRab tracers, at least in the comparison field. This is not an unreasonable assumption to make given the earlier successful RR Lyrae modelling attempts, though with admittedly smaller datasets (e.g. Watkins et al. 2009; Sesar et al. 2010, 2011).

Simple stellar number count models of the halo are based on the following formalism. The heliocentric distance D and galactic coordinates (l, b) of a star and its Galactocentric Cartesian coordinates are related as

$$\begin{aligned} X &= D \cos(l) \cos(b) - R_{\odot} \\ Y &= D \sin(l) \cos(b) \\ Z &= D \sin(b) \\ r^2 &= X^2 + Y^2 + Z^2 q_H^{-2} \end{aligned}$$

where q_H describes the flattening of the halo. Here R_{\odot} is the Sun’s distance from the Galactic center and r is the star’s Galactocentric ellipsoidal distance. The Sun is at $(X, Y, Z) = (-8, 0, 0)$ kpc, the X-axis points towards the Galactic center, Y component in the direction of Galactic rotation and the Z-axis points toward the north Galactic pole.

The stellar density distribution in the inner halo (within

~ 20 kpc) appears to be well described with a simple power-law form

$$\rho_{model}^{RR}(D, l, b) = \rho_{\odot}^{RR} \left(\frac{R_{\odot}}{r} \right)^{\alpha}. \quad (1)$$

At larger distances, a steeper power-law index is required to fit the data well (see e.g. Deason et al. 2011), therefore leading to an overall broken power-law model with characteristic “break radius” r_b

$$\rho_{model}^{RR}(r) = \rho_{\odot}^{RR} \left(\frac{R_{\odot}}{r_b} \right)^{\alpha_{in}} \times \begin{cases} \left(\frac{r_b}{r} \right)^{\alpha_{in}} & \text{if } r \leq r_b, \\ \left(\frac{r_b}{r} \right)^{\alpha_{out}} & \text{if } r > r_b. \end{cases} \quad (2)$$

For a given density model, we can estimate the number of RR Lyrae in the given solid angle within an increment of heliocentric distance ΔD_{RR} around D_{RR}

$$\Delta N_{exp}(D_{RR}, l, b) = \rho_{\odot}^{RR} D_{RR}^2 \rho_{model}^{RR}(D_{RR}, l, b) \cos b \Delta D_{RR} \Delta l \Delta b, \quad (3)$$

where ρ_{\odot}^{RR} is number density of RRab in the solar neighborhood.

As the CSS RRab catalogue is incomplete, with the completeness dropping at faint magnitudes from under 70% to under 40%, we need to scale down the model predictions (and more so at large distances) to take the survey detection efficiency into account. The fraction of RR Lyrae detected by the CSS as a function of magnitude is presented in Figure 13 of DR13a. The insert of Figure 1 shows the completeness as a function of heliocentric distance. This curve is derived from Figure 13 of DR13a, using the well-known relation between apparent magnitude and distance modulus and assuming $M_V = 0.6$:

$$D_{RR} = 10^{0.2(V - M_V + 5 - A_V)} \quad (4)$$

where $V_0 = V - A_V$ is the average magnitude from the Fourier fit to the RRab light curves listed in Table 1 of DR13a and Table 2 of DR13b. The efficiency-corrected number of stars predicted by the model is thus given by

$$\Delta N_{obs}(D_{RR}, l, b) = F(D_{RR}) \Delta N_{exp}(D_{RR}, l, b) \quad (5)$$

where F is the completeness function shown in Figure 1. The efficiency curve needs to be shifted in distance as A_V varies.

Rather than fitting our own density model ρ_{model} to the CSS RR Lyrae data we have re-used some of the halo model parameters obtained in earlier studies.¹ Table 1 lists the best-fit values for the number density distribution of different halo tracers: main-sequence stars (Sesar et al. 2010); RRab Lyrae between 5 and 23 kpc (Sesar et al. 2013); and blue horizontal branch stars (Deason et al. 2011). Also displayed are the values obtained in two independent studies of the RR Lyrae density distribution in Stripe 82 (Watkins et al. 2009; Sesar et al. 2010). All normalisation values ρ_{\odot}^{RR} listed in Table 1 are estimated for the Milky Way halo RRab stars. Some of these were obtained using the actual RR

Lyrae tracers, for example those by Watkins et al. (2009) and Sesar et al. (2010) detected in the SDSS Stripe 82 data and the LINEAR II catalogue (Sesar et al. 2013). However, in two out of five modeling efforts, stars other than RR Lyrae were employed. For the BPL model fit to MS stars from the Canada France Hawaii Telescope Legacy Survey, Table 1 gives the conversion of the density normalisation to RR Lyrae counts derived by Sesar et al. (2013).

For the BPL model of Deason et al. (2011) derived using BHB stars, the RR Lyrae density normalisation is obtained using the following procedure. The model of Deason et al. (2011) and the CSS RRab data are both integrated over the area covered by the control field shown in blue in Figure 1. The control field is a $1,100 \text{ deg}^2$ region with $0^\circ < l < 80^\circ$ and $45^\circ < b < 70^\circ$. To our knowledge, there are no stellar streams or satellites reported in this area within distances $D_{RR} < 30$ kpc. Equating the incompleteness-corrected integral of the BPL model of Deason et al. (2011) over the control field area out to $D = 30$ kpc to the total number of RRab in the CSS data we obtain $\rho_{\odot}^{RR} = 7.3 \text{ kpc}^{-3}$, shown in italics in Table 1.

Figure 2 compares the CSS RRab data in the control field and the predictions of the five simple power-law models listed in Table 1. The data is shown in the blue histograms using 2 kpc binning (errors on the distance are $\sim 7\%$, i.e. less than the bin size). The uncertainty in the number of expected RR Lyrae is calculated as $\delta N_{obs} \approx \sqrt{(\delta N_{exp})^2 + (\delta F)^2}$, where δF is the uncertainty in the completeness estimated in each distance bin and δN_{exp} is the Poisson uncertainty $\sqrt{N_{exp}}$. According to the Figure, single power-law models can not reproduce the data adequately. In order not to over-estimate the number of tracers at large distances, SPL models must under-predict the counts at smaller distances: note how both red dashed and dash-dotted curves fall low in the distance range $5 < D < 15$ kpc. Of the three broken power-law models, the ones by Deason et al. (2011) and Sesar et al. (2011) perform the best with the model of Watkins et al. (2009) consistently over-predicting RR Lyrae counts at $D > 10$ kpc, albeit at the level $< 10\%$ ². In what follows, we choose to compare the data with the model of Deason et al. (2011) simply because it gives marginally higher RRab counts at $D > 10$ kpc, and therefore compared to the prediction of Sesar et al. (2011) the estimate of sub-structure excess is slightly less optimistic.

4 RR LYRAE IN THE HERCULES-AQUILA CLOUD

Figure 3 gives the all-sky density distribution of RR Lyrae with $10 < D < 25$ kpc in the CSS and in the model of Deason et al. (2011) applying the re-normalisation deduced in the previous section. The left (data) and the middle (model) columns of the Figure look very similar, and as illustrated in the right panel (residuals), the agreement is only broken in the few regions dominated by the known halo sub-structures. More precisely, at $-100^\circ < l < -50^\circ$ and $b > 30^\circ$, the Virgo Cloud, i.e. the nearer portion of

¹ For a discussion of the difficulties of fitting a smooth density distribution to an RR Lyrae dataset, see section 7 of Sesar et al. (2013).

² Note that the (Watkins et al. 2009) model has to be scaled down by a factor of 11 in agreement with DR13b.

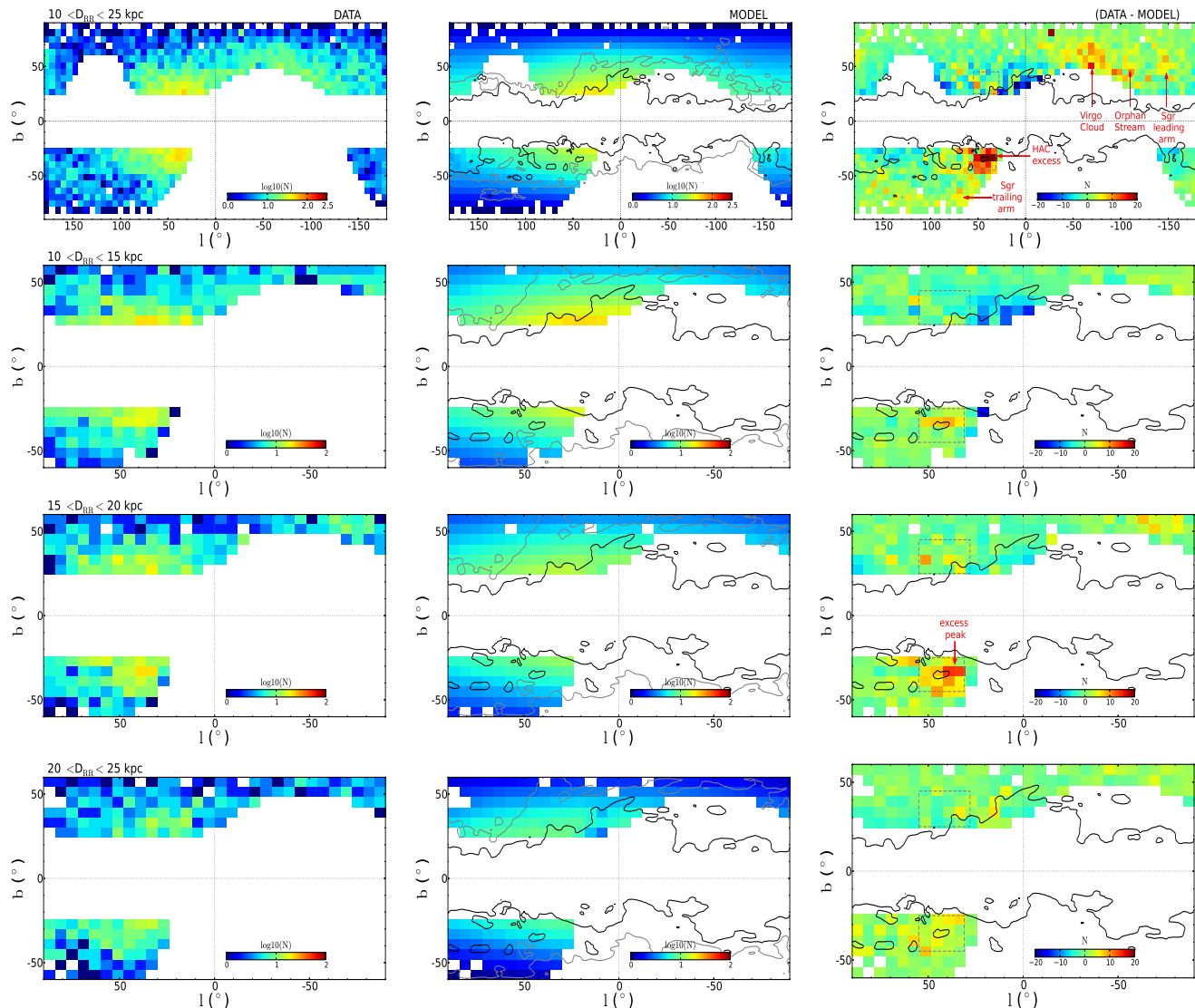


Figure 3. Data, model predictions and residuals (left, middle and right panels respectively) in Galactic coordinates, in $6^\circ \times 6^\circ$ bins. The number density map was not smoothed and it takes into account the efficiency correction at varying l and b . Overlaid on the plots are contours of constant reddening $E(B-V)$ (black is $E(B-V) = 0.10$ and gray is $E(B-V) = 0.04$). Top panels: all-sky density distribution of RR Lyrae with $10 < D_{RR} < 25$ kpc in the CSS (left) and the model Deason et al. (2011) (middle). The residuals (right) highlight the halo substructure, in particular the Virgo Cloud (possibly mostly the VSS), the Orphan Stream, and the Sagittarius stream. A strong excess of RR Lyrae is present in the SH region. Lower panels: zoom-in density maps of the central 180° of the Galaxy in three distance bins: $10 < D_{RR} < 15$ kpc (2nd row), $15 < D_{RR} < 20$ kpc (3rd row) and $20 < D_{RR} < 25$ kpc (4th row). The peak of the excess in the SH field is located in the $15 < D_{RR} < 20$ kpc distance bin, as also shown in Figure 4. Note that the left and middle panels show the logarithm of the stellar number density in each 6×6 deg 2 bin.

it, the VSS (see e.g. Zinn et al. 2014) can be clearly seen connecting to the leading tail of the Sgr stream. In-between these two large structures, at approximately constant Galactic latitude (at the resolution of the map) $b \sim 50^\circ$ runs the narrow Orphan Stream. The Sgr trailing tail is under the disk, at $50^\circ < l < 180^\circ$ and $b < -60^\circ$. Comparing the RRab density in the Galactic North and South at $30^\circ < l < 50^\circ$, an excess at $-50^\circ < b < -20^\circ$ is obvious, roughly bounded by the SH on-cloud field. While the top row gives the distribution of RRab at all distances over the whole sky, the second, third and fourth row of the Figure zoom-in on the central 180° in the Galaxy and map the RRab in three distance bins: $10 < D < 15$ kpc, $15 < D < 20$ kpc and $20 < D < 25$

kpc. Judging by the evolution of the stellar density in the residual map inside the SH on-cloud field, the peak of the HAC is clearly located in the $15 < D_{RR} < 20$ kpc distance range, as also shown in Figure 4. In the North, the RR Lyrae overdensity strength in the on-cloud field is greatly reduced as compared to the South. It is quite possible that the HAC is asymmetric with respect to the plane of the disk. However, there could be a more prosaic explanation for such an observation. Grey contours in the Figure 3 reveal the levels of the dust extinction in the Galaxy as deduced by Schlegel et al. (1998). According to this map, the reddening is patchy on rather large angular scales. In particular, a spur of dust reaches up to higher Galactic latitudes in the

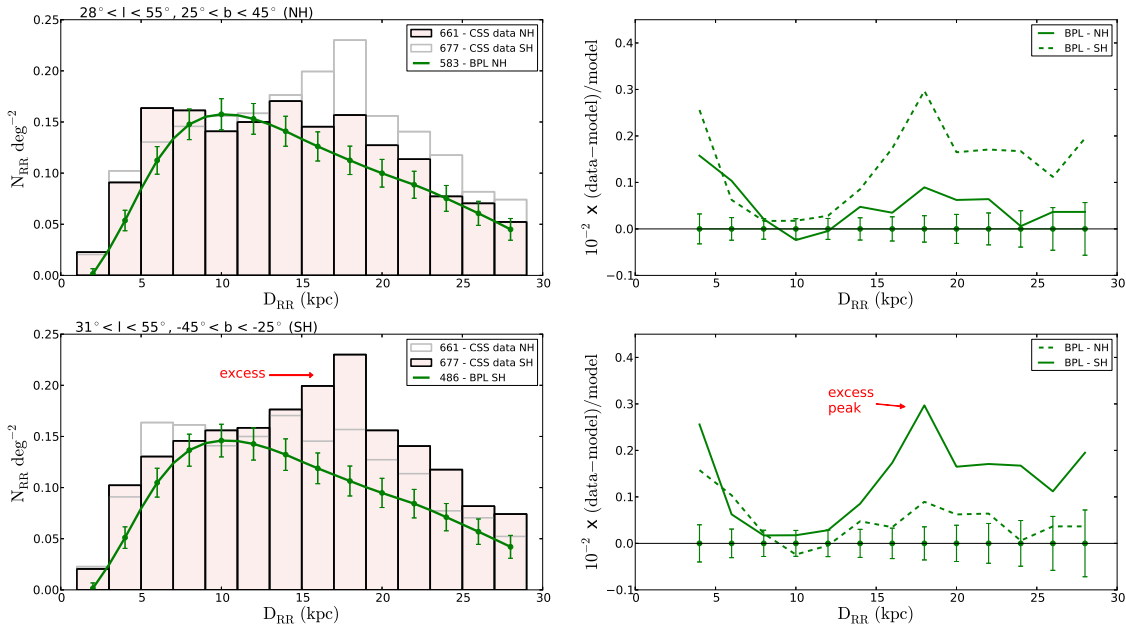


Figure 4. Left panels: heliocentric distance number density distribution for CSS R Rab in bins of 2 kpc and Deason et al. (2011) model predictions with error bars (in green), completeness-corrected, in the NH and SH fields (red selection in Figure 1). Right panels: Residuals between the data and the model. The star density distributions are asymmetric in the NH and SH fields, with a strong excess of stars in the SH between 12 and 25 kpc and a peak at ~ 18 kpc, also revealed in Figure 3. The excess in the NH field is weaker and not particularly significant taking into account the large error bars (see legend for plot labels).

Northern hemisphere. Therefore, this extra extinction could be responsible for diminished star counts in the NH field. Clearly, the extinction by dust plays some role in shaping the apparent stellar halo density at lower Galactic l and b as illustrated in the top right panel of the Figure, where an *under-density* is observed directly above the bulge, falling neatly inside the reddening contours.

According to previous studies (e.g. Belokurov et al. 2007; Watkins et al. 2009), the HAC is situated in the range $20^\circ < l < 80^\circ$, matching closely our detection in the Galactic South. To investigate in detail the line-of-sight distribution of R Rab stars in the Cloud, we focus on two fields in the inner Galaxy, one in the Northern Hemisphere (NH: $28^\circ < l < 55^\circ, 25^\circ < b < 45^\circ$) and one in the Southern Hemisphere (SH: $31^\circ < l < 55^\circ, -45^\circ < b < -25^\circ$). These fields are marked in red in Figure 1. Figure 4 shows the heliocentric distance number density distribution of R Rab in the NH (top) and SH (bottom) fields together with the model predictions in the left column, and the relative residuals between the data and the model in the right column. The errors on the predicted number of RR Lyrae δN_{obs} as a function of distance have been estimated as in the previous section, and take into account the uncertainty in the completeness δF and in the expected number of counts δN_{exp} . As evidenced in the top left panel, overall the R Rab distribution is in reasonable agreement with the model, although it exceeds the predicted counts slightly, especially at $15 < D < 20$ kpc. As the lower panel of Figure 4 illustrates, in the Southern on-cloud field, SH, there exists a strong over-abundance of R Rab stars. The data exceeds the model at all distances beyond 10 kpc, however the observed distribution shows a clear peak in the 17-19 kpc distance bin.

To further investigate the extent of the Cloud, Figure 5 presents the Galactic plane projections of the density of stars

with $10 < D < 30$ kpc in the three regions containing the control field ($0^\circ < l < 85^\circ, 45^\circ < b < 70^\circ$, top row), the NH and NH2 fields ($0^\circ < l < 85^\circ, 25^\circ < b < 45^\circ$, middle row), as well as the SH and SH2 fields ($31^\circ < l < 85^\circ, -45^\circ < b < -25^\circ$, bottom row). The data is shown in the Left, the model predictions in the Middle and the residuals in the Right panels. The top panels confirm that the Deason et al. (2011) model is able to reproduce the broad-brush features of the data in the control-field, as also seen in Figure 2. In the middle panels, an under-density is visible at low Galactic latitudes at $l < 30^\circ$ (most likely caused by the unaccounted dust extinction) as described above. However these also reveal a small excess for $28^\circ < l < 55^\circ$ and $R > 12$ kpc. Finally, the most dramatic over-density of R Rab stars is located below the Galactic plane, at the projected heliocentric distances between 12 and 16 kpc, for $30^\circ < l < 50^\circ$ as evident from the maps shown in the bottom panels.

4.1 Oosterhoff dichotomy in the North and the South fields

The RR Lyrae period-amplitude plane is not populated uniformly. There appears to be significant clumping in the distribution, also known as the Oosterhoff dichotomy (Oosterhoff 1939). This bimodality, most pronounced for members of the Galactic star clusters, is suspected to originate mostly from the metallicity differences amongst the population (see e.g. a review by Catelan 2009). The Oosterhoff I (Oo I) type globular clusters ($< P_{ab} > \sim 0.55$ days) are more metal-rich compared to the Oosterhoff II (Oo II) globular clusters ($< P_{ab} > \sim 0.64$ days). One hypothesis is that Oo II type clusters formed early in the proto-Galaxy while Oo I type clusters might have formed some 2 to 3 Gyrs later (e.g. Lee & Carney 1999). However, GC ages measured with the help

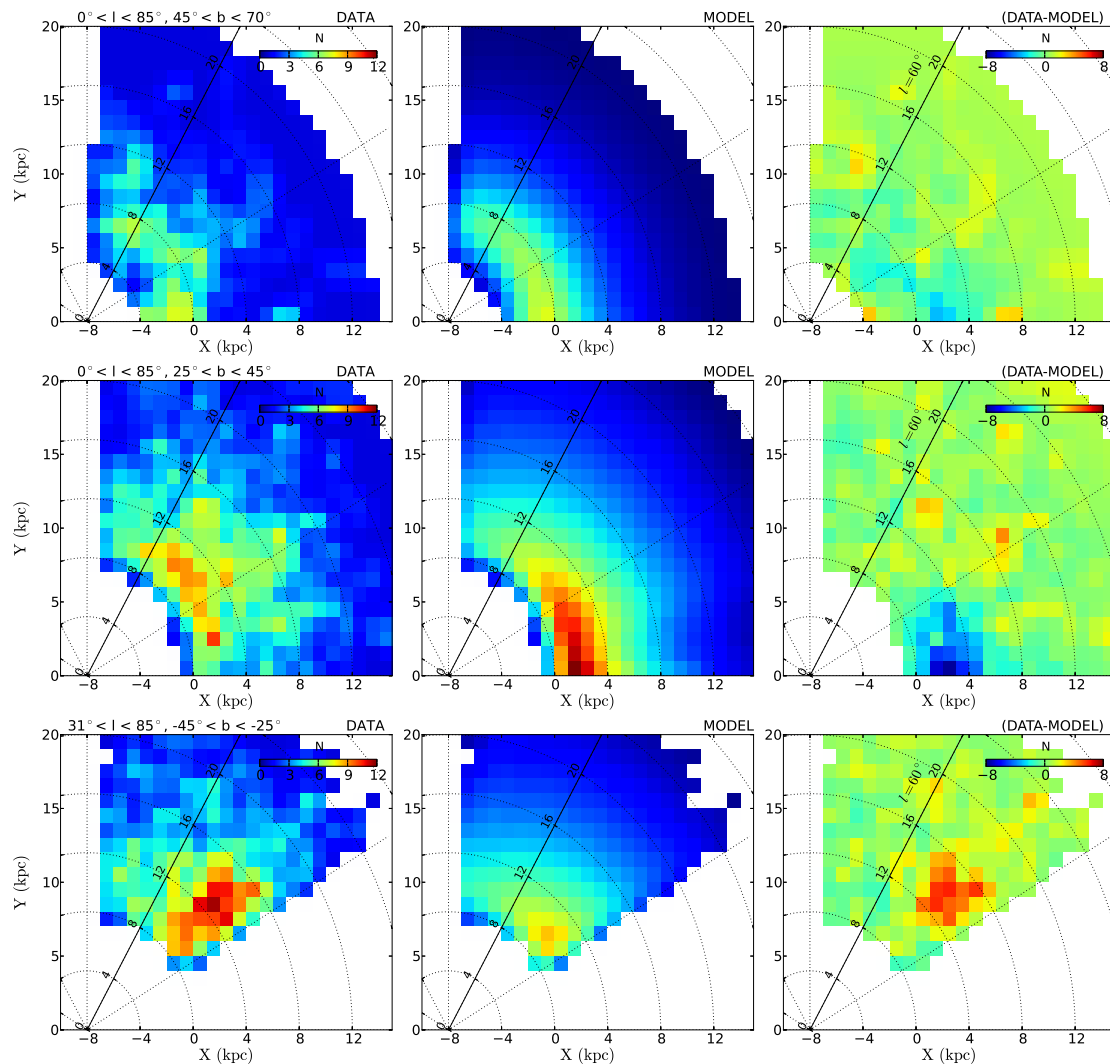


Figure 5. Top panels: X-Y number density maps over a 1132 deg^2 field for the data (left) and the model (middle) in the control-field outlined in blue in Figure 1. These maps indicate the good agreement between the data and the model in this region of the sky where no known halo substructure is present in the distance range considered. Middle panels: X-Y maps over a 1385 deg^2 field that includes our selection of the NH and NH2 fields. We see a small overdensity at $30^\circ < l < 50^\circ$ but also a strong under density for $l < 20^\circ$, which is due to the incompleteness of the survey in a region of high extinction, as shown by the black contours of constant $E(B-V)$ reddening in Figure 3. Lower panels: X-Y map over a 880 deg^2 region which includes the SH and SH2 fields. The residuals reveal the RRL excess in the SH at projected distances on the Galactic plane between 12 and 16 kpc. The maps have been smoothed with a $\sigma = 0.6$ Gaussian filter and are limited to the $10 < D < 30$ kpc distance range. The origin marks the location of the Galactic center (the Sun is at $X = -8$; $Y = 0$ kpc).

of HST ACS photometry (e.g. Dotter et al. 2010) reveal that the age differences might be substantially smaller. Many of the neighbouring dwarf spheroidal galaxies and their globular clusters do not display the Oosterhoff dichotomy but fall instead in the so-called Oosterhoff gap on the period-amplitude (Bailey) diagram with $0.58 < P_{ab} < 0.62$ days. It is therefore clear that the distribution of lightcurve properties of the Galactic RR Lyrae contains complementary information about the accretion history of the stellar halo itself harboring a larger fraction of Oo I type stars (e.g. Catelan & Cortés 2008).

The two top panels of Figure 6 show the so-called Bailey diagrams for CSS RRab with heliocentric distances between 12 and 22 kpc in the NH and SH fields (c.f. Figure 3 in the previous section). We trace the loci for Oo I and Oo II type

globular clusters (blue and magenta lines respectively) using the period-amplitude relation defined by Zorotovic et al. (2010) and determine the period shifts $\Delta P(A)$ (i.e. the offset in period at constant amplitude from the Oo I locus line) for each RRab. In the bottom panels of Figure 6 we show the ΔP period-shift distribution for the RRab stars in the NH ($28^\circ < l < 55^\circ$, $25^\circ < b < 45^\circ$, left) and in the SH ($31^\circ < l < 55^\circ$, $-45^\circ < b < -25^\circ$, right) fields. The distribution of ΔP values is centered on $\Delta P = 0$ by definition (the position of the Oo I locus). However a tail at long periods is noticeable; this is due to the Oo II component. By fitting the period shift distribution with a two-component Gaussian model we estimate that in the NH field, $\sim 69\%$ of type-ab RRL belong to the Oo I component and 31% to the Oo II in the distance range considered (left panels, Figure 6). In

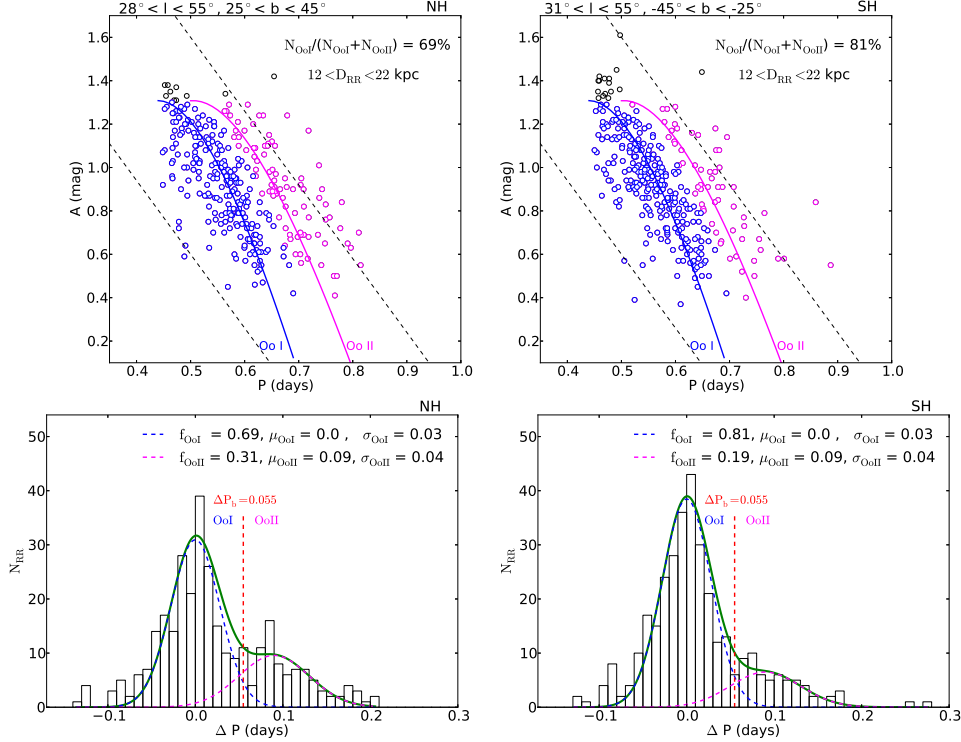


Figure 6. Top panels: Bailey diagrams for the RRL in the NH and SH fields, at $12 < D < 22$ kpc. The continuous lines indicate the loci for the Oo I and Oo II components as defined by Zorotovic et al. (2010). Blue and magenta indicate the Oo I and Oo II RRL respectively, tentatively classified using the $\Delta P = 0.055$ boundary. The dashed black lines represent the lower ($A = 2.3 - 3.4P$) and upper ($A = 3.3 - 3.4P$) limits expected for most of the RRL. Bottom panels: Histogram of the period shifts calculated for each RRL at constant amplitude from the Oo I locus (blue line in the top panels) in the period-amplitude plane defined by Zorotovic et al. (2010). In the NH field 69% of the stars are Oo I type while in the SH, 81% of them. The expected proportion of Oo I RRL is $\sim 75\%$. See the text for more details.

the SH field the proportion is significantly different, with the majority of RRL (81%) belonging to Oo I population and only 19% to the Oo II population (right panels, Figure 6). To split the sample into Oo I and Oo II populations a simple boundary at constant period-shift of $\Delta P = 0.055$ (red line in the bottom panels) is used: Oo I type lie to the left of the boundary and Oo II type to the right. In the Bailey diagrams (top panels in Figure 6) for the NH and SH fields the Oo I and Oo II types RRL are marked with blue and magenta respectively while black indicates the stars that failed this simple classification, because situated above the defined loci. Previous studies (e.g. Miceli et al. 2008; Sesar et al. 2013; Drake et al. 2013a) have shown that $\sim 75\%$ of halo field RRL belong to the Oo I population. The fact that the SH field contains $\sim 81\%$ of these indicates that the progenitor of the HAC in the Southern Hemisphere is either an Oo I population globular cluster or a dwarf galaxy falling into the Oosterhoff gap. In fact, using the boundary $\Delta P = 0.055$ we classify most of the stars in the Oosterhoff gap as Oo I type. Type ab stars that lie to the left of the Oo I curve may either be metal-rich or have smaller mean amplitudes because of the Blazhko effect (Blazhko 1907).

We show the spatial distribution of the Oo I and Oo II components along the sight-lines towards the HAC region in Figure 7. The density map is shown in the plane of heliocentric distance $R = \sqrt{X^2 + Y^2}$ and height above the plane Z for both NH (for this plot, $31^\circ < l < 55^\circ$ instead

Table 2. Poisson Statistics for the RRL in the HAC region, shown in the top panels of Figure 7. We list two values for each region: RRL with $0 < R < 10$ kpc / $10 < R < 20$ kpc. The 'NH' field has $0 < Z < 15$ kpc while the 'SH', $-15 < Z < 0$ kpc.

RRL Type	Region	N_{exp}	N_{data}	Significance
Oo I, II	NH	223/247	234/300	0.74/3.37
Oo I, II	SH	223/247	241/368	1.21/7.70
Oo I	NH	168/185	179/221	0.85/2.65
Oo I	SH	168/185	168/307	0.00/8.97
Oo II	NH	56/62	55/79	0.13/2.16
Oo II	SH	56/62	73/61	2.27/0.37

of $28^\circ < l < 55^\circ$, to allow for symmetry with the SH field) and SH fields. The left column shows the observed number density distributions of the RR Lyrae, the middle column gives the smooth model predictions and finally the right panels report the resulting residuals. From top to bottom the rows show: the entire RR Lyrae sample (top); the Oo I type (middle); and the Oo II type (bottom). The model density normalisations for the individual Oo types are chosen by simply assuming that Oo I types make up 75% of the total RRL population and Oo II the remaining 25%. The residual maps (right panels) reveal asymmetries in the North-South distributions. We quantify the statistical significance of the overdense regions relative to the model for the (Oo I + Oo

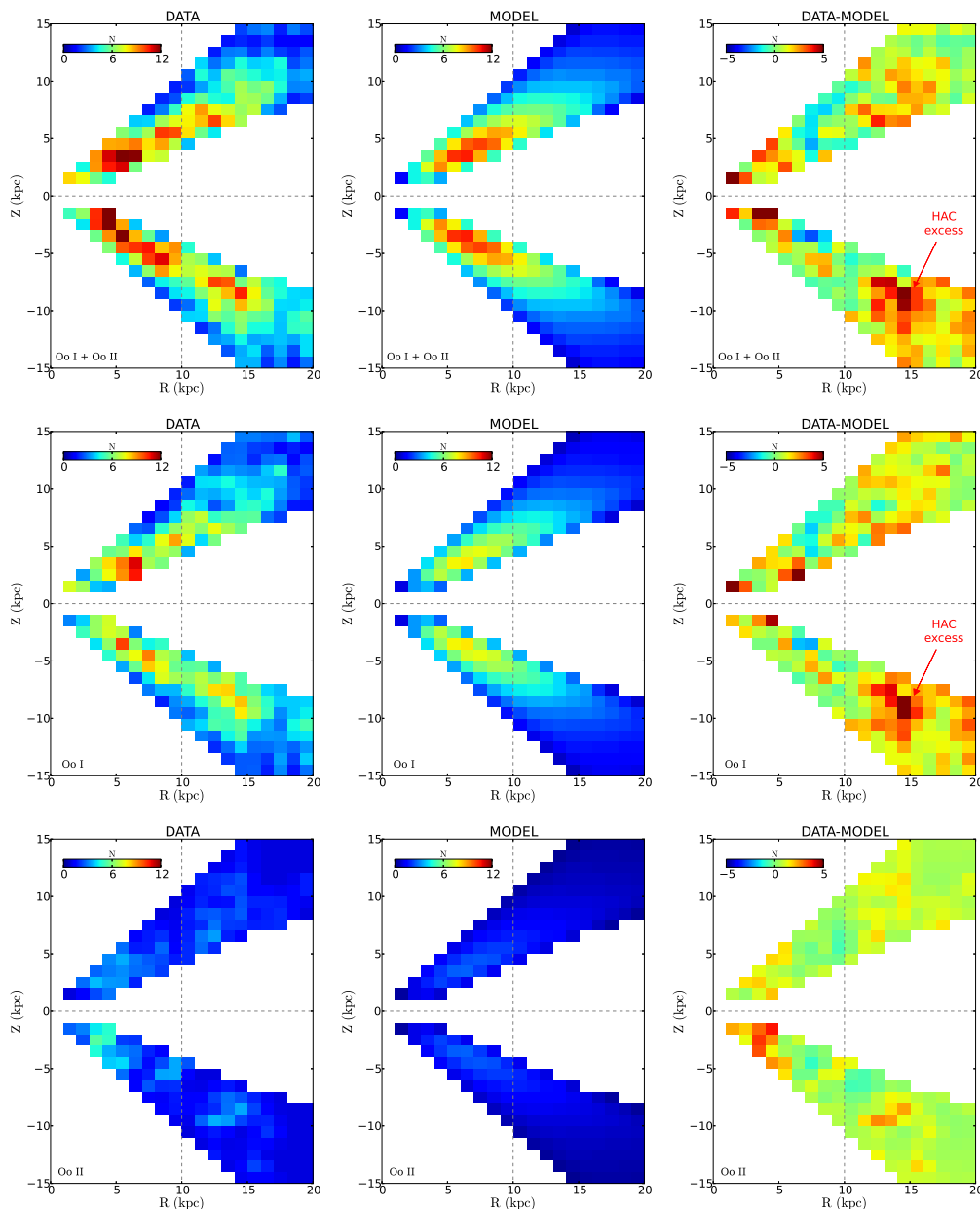


Figure 7. R vs Z number density maps of all the RRab Lyrae (top row), Oo I RRL (middle row) and Oo II RRL (bottom row) for the data (left column) and the Deason et al. (2011) model (middle column) in the N-S symmetric fields $31^\circ < l < 55^\circ$, $|b| < 45^\circ$. The residual maps (right column) reveal an overdensity of Oo I RRab in the Southern Hemisphere, for $R > 10$ kpc. A much weaker signal is present also in the Northern Hemisphere for $R > 12$ kpc, as already seen in Figure 5. The model calculations take into account the completeness function of the survey. The bin size is 0.5 kpc x 0.5 kpc. The statistical significances of the overdense regions are listed in Table 2. The plots have been smoothed with a Gaussian kernel of $\sigma = 0.6$.

II), Oo I and Oo II populations at heliocentric distances R smaller and greater than 10 kpc. For each population we compute the statistical significance by finding the absolute difference between the observed (N_{data}) and expected (N_{exp}) number of RR Lyrae stars, then dividing it by the Poisson uncertainty ($\sqrt{N_{exp}}$). The results of this analysis are summarized in Table 2. We list separately the values for the regions above (NH) and below (SH) the Galactic plane (see column 'region') and for each region we compute the significance of the overdensity for $R < 10$ kpc and $R > 10$ kpc (we list two values in each column). The values confirm that the model agrees with the data for $R < 10$ kpc, while there is

a significant excess of RRL (more specifically Oo I type) for $R > 10$ kpc. The excess has a statistical significance of $\sim 9\sigma$ for the Oo I population and $\sim 8\sigma$ if we consider the whole sample. While in the SH the overdensity seems to be due to the Oo I population, in the NH there seems to be a small excess due to both the Oo I ($\sim 2.6\sigma$) and Oo II populations ($\sim 2.2\sigma$). These values explain the ratios ($f_{OoI} = 69\%$ for SH and $f_{OoI} = 81\%$ SH) we obtained in Figure 6. Highlighted in black are the values for the Oo I component in the SH. Our results are broadly consistent with those reported in earlier studies. For example, in Figure 24 in Sesar et al. (2010), the Hercules-Aquila Cloud is seen at $310^\circ < R.A. < 330^\circ$ in the

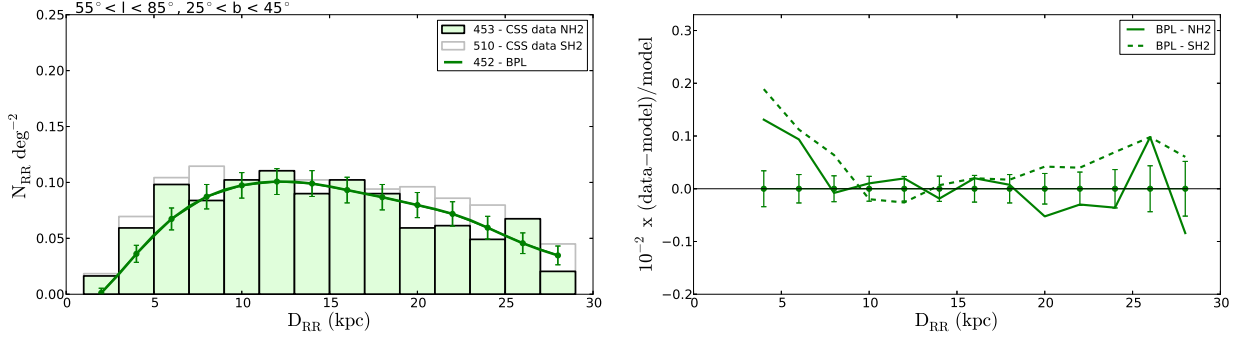


Figure 8. Number density distributions of CSS RRab in the fields NH2 and SH2 adjacent to the NH and SH fields (see Figure 1). The Deason et al. (2011) model agrees with the observed distribution. The absence of a significant overdensity in these regions suggests that the HAC extends mainly to the NH and (mostly) SH fields.

distribution of main-sequence stars in Stripe 82, at distances in the range 10-25 kpc, with a factor of ~ 1.6 overdensity. In the same study, it is found that the HAC is dominated by Oo I stars (end of section 4.5, Sesar et al. (2010)).

4.2 Luminosity of the progenitor

To estimate the total luminosity of the Cloud we need to constrain its spatial extent. Figure 8 shows the heliocentric number density distribution of RRab stars in two regions symmetric with respect to the Galactic plane, and neighbouring the NH and SH fields (note boxes marked in green and labelled NH2 and SH2 in Figure 1). Field NH2 encompasses stars with $55^\circ < l < 85^\circ$, $25^\circ < b < 45^\circ$, while field SH2 contains stars with $55^\circ < l < 85^\circ$, $-45^\circ < b < -25^\circ$. These distributions show no clear excess. Therefore, we can conclude that at the Galactic latitudes probed by the CSS, the HAC members are predominately located in the NH and SH fields.

Assuming that within the CSS footprint the majority of stars belonging to the Cloud are concentrated in the NH and SH fields, it is possible to compute a rough estimate of the initial luminosity of the progenitor. We count the excess RRab stars in both the NH and SH fields with respect to the BPL model, in the 10 to 28 kpc distance range. In the North, this amounts to 76 RRab, and more than double, i.e. 181 RRab stars in the South. The luminosity of the progenitor is then estimated for a range of disruption scenarios. For example, the parent of the Cloud might have been an old and evolved system, with stellar populations similar to that of a globular cluster, packed with numerous RR Lyrae. Alternatively, it could have been a system with an intermediate age population and a smaller proportion of RRL given the total luminosity. In Table 3 we list a series of possible progenitor systems indicating the number of RRab N_{RR}^{sys} in each one, their luminosity L_{sys} and the inferred luminosity of the HAC's progenitor L_{HAC} , assuming:

$$L_{HAC}/N_{RR}^{HAC} = L_{sys}/N_{RR}^{sys} \quad (6)$$

where $N_{RR}^{HAC} = 367$, counting for a $\sim 70\%$ completeness of the survey. The total absolute magnitude of a system, knowing its luminosity is $M_V^{sys} = M_\odot - 2.5 \log_{10}(L_{sys}/L_\odot)$. According to Table 3, the luminosity of the progenitor could be anywhere between $M_V^{HAC} \approx -9$ and $M_V^{HAC} \approx -14$. However, we have assumed a constant 70% completeness

Table 3. Examples of old and intermediate systems and estimates of the luminosity of the HAC progenitor. The values in the first three columns are from Clement et al. (2001) (updated catalogue of Variable Stars in Globular Clusters), Harris (1996, 2010) (the 2010 revision of his Catalog of Parameters for Milky Way Globular Clusters), and Table 1 in Smith et al. (2009) (RRL properties of Dwarf Spheroidal Galaxies).

Old pop. GCs	N_{RR}^{sys}	M_V^{sys}	L_{sys} (L_\odot)	L_{HAC} (L_\odot)	M_V^{HAC}
N5272 (M3)	187	-8.9	$3 \cdot 10^5$	$6 \cdot 10^5$	-9.6
N3201	72	-7.4	$8.1 \cdot 10^4$	$4 \cdot 10^5$	-9.2
N6333(M9)	9	-7.9	$1.3 \cdot 10^5$	$5 \cdot 10^6$	-12
Interm. pop. Dwarf galaxies					
Leo I	47	-12.0	$5.4 \cdot 10^6$	$3 \cdot 10^7$	-14.2
Draco	214	-8.8	$2.8 \cdot 10^5$	$5 \cdot 10^5$	-9.4
Carina	54	-9.1	$3.7 \cdot 10^5$	$3 \cdot 10^6$	-11.2
Fornax	396	-13.4	$1.9 \cdot 10^7$	$2 \cdot 10^7$	-13.3

at all distances while the completeness decreases down to 40% at 30 kpc, leading us to underestimate the actual number of RRL. It is also possible that the HAC is not limited to the NH and SH fields: if the NH and SH overdensities are associated, it is likely that the overdensity extends at lower galactic latitudes. The total luminosity of the Cloud $M_V^{HAC} = -13$ estimated by Belokurov et al. (2007), is in agreement with the results found in this section.

5 CONCLUSIONS

We have used a sample of $\sim 14,000$ RR Lyrae from the Catalina Schmidt Survey to map out the Hercules Aquila Cloud located on the other side of the Galaxy. To illustrate the location and the extent of the Cloud, a schematic drawing of the Cloud's signal as traced by the RR Lyrae is given in Figure 9. The figure gives a graphical summary of the results presented in this Paper, which are also detailed below.

- In the Galactic Southern hemisphere, there is a prominent overdensity of RRab stars in the direction coincident with the previous detections of the Hercules-Aquila Overdensity (see e.g. Belokurov et al. 2007; Watkins et al. 2009).

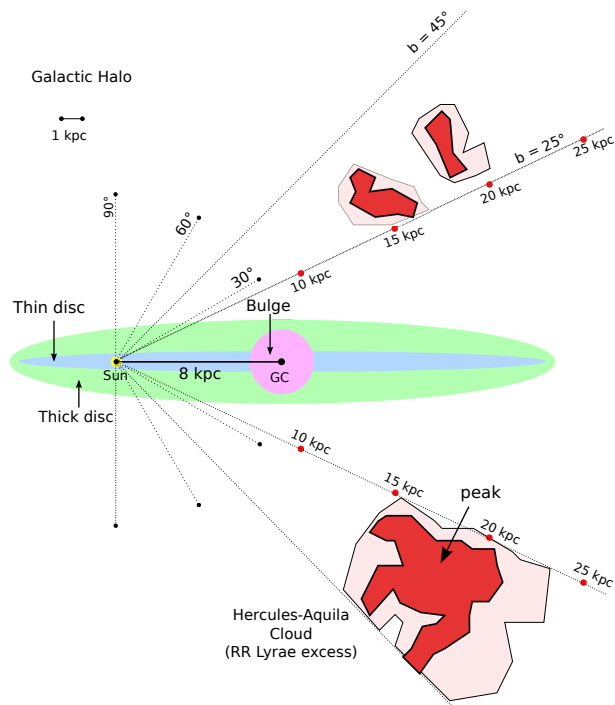


Figure 9. Schematic view of the Milky Way structure. We show two isodensity contours of the Hercules-Aquila Cloud as revealed by the CSS RR Lyrae sample (see also Figure 7). The peak of the RRL over-density is at distances Z between -7 to -13 kpc below the Galactic plane, therefore we confidently exclude that the HAC is a thick disc structure or originated from a bar-disc interaction.

The significance of the RR Lyrae overdensity in the South is $\sim 8\sigma$.

- In the Galactic Northern hemisphere, the excess is barely noticeable. It is therefore possible that the HAC is not symmetric with respect to the disk plane. However, we suspect that the northern signal is greatly reduced by the interstellar dust reaching to higher latitudes above the disk. Without correcting for this the significance of the RR Lyrae overdensity in the North is $\sim 3\sigma$.

- Below the disk, the RR Lyrae excess show a broad peak at $(l, b) \sim (40^\circ, -30^\circ)$ (see Figure 3), while the maximum along the line of sight is reached at a heliocentric of $D \sim 18$ kpc. The portion of the Cloud accessible through the CSS data is at least 20° across. Overall, the physical extent of the Cloud as traced by the RRab stars is at least 4 kpc along each spatial dimension.

- The majority of the RR Lyrae stars contributing to the overdensity are either of Oo I type or fall into the so-called Oosterhoff gap. Therefore, the bulk of the stars in the Cloud progenitor seem to resemble the dominant stellar population of the Galactic halo.

- Using the CSS data we have constrained the pre-disruption luminosity of the HAC progenitor to lie in the range $-15 < M_V < -9$.

Based on the observations outlined above, we conclude that the HAC is indeed a distinct stellar halo sub-structure and not part of the nearby thick disc. Unfortunately, we still lack deep wide-area infrared data to follow the HAC signal to lower Galactic latitudes, and therefore our estimate of the Cloud's extent and luminosity remain rather fuzzy.

Fortunately with the identification of the conspicuous RR Lyrae population in the Cloud reported here, it should now be possible to map the radial velocity across the face of the Hercules-Aquila Cloud and thus illuminate the history of its interaction with the Milky Way.

ACKNOWLEDGEMENTS

We thank Andrew Drake for useful information on the CSS data and the anonymous referee for the illuminating and thorough review. ITS is grateful to Adriano Agnello for his constructive comments and help. This work was partially supported by the Gaia Research for European Astronomy Training (GREAT-ITN) Marie Curie network, funded through the European Union Seventh Framework Programme (FP7/2007-2013) under grant agreement number 264895. The research leading to these results has also received funding from the European Research Council under the European Union's Seventh Framework Programme (FP/2007-2013) / ERC Grant Agreement n. 308024. VB acknowledges financial support from the Royal Society.

REFERENCES

- Belokurov V., 2013, arXiv:1307.0041, 57, 100
 Belokurov V., Evans N. W., Bell E. F., Irwin M. J. et al., 2007, ApJ, 657, L89
 Blažko S., 1907, Astronomische Nachrichten, 175, 327
 Catelan M., 2009, Ap&SS, 320, 261
 Catelan M., Cortés C., 2008, ApJ, 676, L135
 Chaboyer B., 1999, Post-Hipparcos Cosmic Candles, 237, 111
 Clement C. M., Muzzin A., Dufton Q., Ponnampalam T. et al., 2001, AJ, 122, 2587
 Deason A. J., Belokurov V., Evans N. W., 2011, MNRAS, 416, 2903
 Dotter A., Sarajedini A., Anderson J., Aparicio A. et al., 2010, ApJ, 708, 698
 Drake A. J., Catelan M., Djorgovski S. G., Torrealba G. et al., 2013a, ApJ, 763, 32
 Drake A. J., Catelan M., Djorgovski S. G., Torrealba G. et al., 2013b, ApJ, 765, 154
 Duffau S., Zinn R., Vivas A. K., Carraro G., Méndez R. A., Winnick R., Gallart C., 2006, ApJ, 636, L97
 Harris W. E., 1996, AJ, 112, 1487
 Harris W. E., 2010, ArXiv e-prints
 Jurić M., Ivezić Ž., Brooks A., Lupton R. H. et al., 2008, ApJ, 673, 864
 Larsen J. A., Cabanela J. E., Humphreys R. M., 2011, AJ, 141, 130
 Lee J.-W., Carney B. W., 1999, AJ, 118, 1373
 Majewski S. R., Skrutskie M. F., Weinberg M. D., Osthheimer J. C., 2003, ApJ, 599, 1082
 Mateu C., Vivas A. K., Downes J. J., Briceño C., Zinn R., Cruz-Díaz G., 2012, MNRAS, 427, 3374
 Miceli A., Rest A., Stubbs C. W., Hawley S. L. et al., 2008, ApJ, 678, 865
 Oosterhoff P. T., 1939, The Observatory, 62, 104
 Preston G. W., Shtetman S. A., Beers T. C., 1991, ApJ, 375, 121

- Schlegel D. J., Finkbeiner D. P., Davis M., 1998, *ApJ*, 500, 525
- Sesar B., Ivezić Ž., Grammer S. H., Morgan D. P. et al., 2010, *ApJ*, 708, 717
- Sesar B., Ivezić Ž., Stuart J. S., Morgan D. M. et al., 2013, *AJ*, 146, 21
- Sesar B., Jurić M., Ivezić Ž., 2011, *ApJ*, 731, 4
- Smith H. A., Catelan M., Clementini G., 2009, in *American Institute of Physics Conference Series*, Vol. 1170, American Institute of Physics Conference Series, Guzik J. A., Bradley P. A., eds., pp. 179–187
- Vivas A. K., Zinn R., 2006, *AJ*, 132, 714
- Watkins L. L., Evans N. W., Belokurov V., Smith M. C. et al., 2009, *MNRAS*, 398, 1757
- Zinn R., Horowitz B., Vivas A. K., Baltay C., Ellman N., Hadjiyska E., Rabinowitz D., Miller L., 2014, *ApJ*, 781, 22
- Zorotovic M., Catelan M., Smith H. A., Pritzl B. J. et al., 2010, *AJ*, 139, 357